Effect of cooling rate on the microstructure and solidification characteristics of Al2024 alloy using computer-aided thermal analysis technique

M. H. Ghoncheh · S. G. Shabestari · M. H. Abbasi

Abstract The aim of this work was to investigate the effect of different cooling rates on the microstructure and solidification parameters of 2024 aluminum alloy. Solidification characteristics are recognized from the cooling curve and its first and second derivative curves which have been plotted using thermal analysis technique. In this study, a mold having high cooling rate was designed and used to simulate the direct-chill casting process. The results of thermal analysis show that the characteristic parameters of Al2024 alloy are influenced by cooling rate. The cooling rates used in the present study range from 0.4 to 17.5 °C s^{-1}. Increasing the cooling rate affects the undercooling parameters both in liquidus and eutectic solidification regions. Investigations showed that solidification parameters such as nucleation temperature, recalescence undercooling temperature, and range of solidification temperature are influenced by variation of cooling rates. Microstructural evaluation was carried out to present the correlation between the cooling rate and dendrite arm spacing.

Keywords Al2024 alloy · Thermal analysis · Cooling rate · Dendrite arm spacing (DAS) · Direct-chill (DC) casting

M. H. Ghoncheh · S. G. Shabestari (✉) · M. H. Abbasi
Center of Excellent for High Strength Alloys Technology
(CEHSAT), School of Metallurgy and Materials Engineering,
Iran University of Science and Technology (IUST), Narmak,
16846-13114 Tehran, Iran
e-mail: shabestari@iust.ac.ir

Introduction

Al2024 alloy in Al–Cu–Mg alloys system developed to use in aerospace applications due to its low density and good damage tolerance. The high strength in this alloy is primarily derived from the precipitation and redistribution of fine Al$_2$CuMg particles. Typical applications of this alloy include aircrafts structures, rivets, and truck wheels [1, 2].

The casting of extrusion billets and rolling ingots of aluminum alloys such as Al2024 billets has principally been carried out by the direct-chill (DC) casting process. The DC process has been classified into vertical direct-chill (VDC) casting and horizontal direct-chill (HDC) casting process. The cooling rate used in these methods is high, and its range is between 10 and 18 °C s^{-1}. During DC casting, alloy composition and casting parameters are critical for the formation of solidification defects. The main process parameters that can be controlled and affect to a great extent the quality of the billet and its structures are as follows: the casting speed, water flow rate, and melt temperature [3, 4]. To control these parameters, computer-aided cooling curve thermal analysis (CA-CCTA) is a good technique that can be used [5–7].

Thermal analysis is used extensively in casting process to control the quality of the metals. The cooling curve method is useful for commercial applications for a number of reasons: it is simple, inexpensive, and provides consistent results. This technique is a good choice for obtaining fundamental relationship between cooling curve characteristics and melts [6, 7]. An accurate thermal analysis system should be able to quantify parameters such as grain size, dendrite coherency point, level of modification, temperature of intermetallics formation during solidification, solid fraction, and latent heat [8–10]. In most researches, thermal analysis method is used to determine the solidification characteristics of aluminum

casting alloys, but a few researches have been done on wrought aluminum alloys [11]. Assessment of solidification parameters in high cooling rate condition is difficult. The reason is, when a molten metal is solidified by high cooling rate, the latent heat of any reaction in solidification process is released quickly, and reactions peaks in cooling curve and first derivative curve are too hard to be detected. In addition, most of intermetallics in wrought aluminum alloys have a low amount of latent heat in comparison with some compounds such as silicon-rich intermetallics in cast aluminum alloys.

Effect of cooling rate on the structural features of 2000 series alloys has been investigated by some authors [11]. According to their work, increasing the cooling rate refines all microstructural features including grain size, dendrite arm spacing (DAS), and intermetallic phases. Dendrite arm spacing is affected by increasing the cooling rate much more than other microstructural features [12].

Flemings had concluded that increasing the cooling rate improved not only the soundness, but also more significantly affected the refinement in dendritic structure [12]. He presented a correlation for secondary dendrite arm spacing for a wide variety of alloys. These equations were "DAS $= A(t_f)^n$ and DAS $= B(C.R)^{-n}$". In these equations, t_f is the time interval between liquidus and solidus, C.R is cooling rate, A and B are constant, and n is in the range from 0.33 to 0.5 [13–17]. Effect of two cooling rates on 2024 aluminum alloy was studied by Backerud et al. [11] They presented an equation "DAS $= 102.33(C.R)^{-0.33}$" for this alloy. Also Flemings et al. [16] reported "DAS $= 45(C.R)^{-0.39}$ and DAS $= 7.5(t_f)^{0.39}$" equations for Al-4.5 mass% Cu alloy. The main aim of this research was to study the microstructure and solidification parameters of 2024 wrought aluminum alloy. To achieve this purpose, computer-aided cooling curve thermal analysis was used. Microstructure of the alloy was studied at different cooling rates. Also, a numerical equation was proposed to predict cooling rate by measuring DAS in this alloy.

Experimental

Material and melting

Commercial 2024 aluminum alloy was used in this research. Its chemical composition is given in Table 1. Seven types of molds having different cooling rates were used to investigate the influence of cooling rate on the solidification characteristics. To simulate the direct-chill casting process which has high cooling rate condition, water circulated steel mold was designed. The dimensions of the mold are shown in Fig. 1. 500 g of Al2024 alloy was melted in an electric resistance furnace in each experiment, and the melt was maintained at a

Table 1 Chemical composition of 2024 aluminum alloy

Alloy composition	Elements/mass%					
	Cu	Mg	Mn	Fe	Si	Al
Al2024 alloy	4.33	1.45	0.63	0.23	0.16	Bal.

temperature of 750 ± 10 °C. The melt was degassed with nitrogen-base degasser capsule for 5 min and was regularly stirred to achieve a homogenized melt. After melting, the oxide layer was skimmed from the surface and the molten metal poured into the mold. Samples were solidified in wide range of cooling rates from 0.4 to 17.5 °C s^{-1}. In each cooling rate, three samples were cast, in order to check the reproducibility and the accuracy.

Thermal analysis

Cooling curve thermal analysis was performed on all samples using K-type thermocouples (chromel–alumel) manufactured by OMEGA engineering company (OMEGA Engineering Inc, Stanford, Connecticut, USA). It was inserted into a stainless steel sheath and connected to a high-speed data acquisition system. The signal was recorded each 0.1 s for all experiments. The thermocouples were located at exactly the same depth in the melt (at a location of 20 mm from the bottom of the mold). Analog to digital (A/D) convertor used in this work has a sensitive 16-bit convertor (resolution of $1/2^{16}$ or 0.0015 %), response time of 0.02 s, and high accuracy detection. Thermal analysis program can simultaneously display the cooling curves, temperature, and time on the monitor of the computer for an instant observation. Each test was repeated at least three times. Time–temperature data (the variation of temperature with time) were recorded with the frequency of 10 readings per second and plotted using Origin pro.8.6 software (Origin Lab Corporation, Northampton, MA). The adjacent averaging method over 20 points was applied to each data to smooth the thermal analysis curves. Before each series of tests, the thermocouples were calibrated with melting and solidification of high purity aluminum (99.99 mass% Al). The processing included smoothing, curve fitting, plotting the first derivatives, identifying the onset and end of solidification, determining solidification parameters such as cooling rate, nucleation temperatures, recalescence undercooling, solidification range, and total solidification time. There are some differences in defining the thermal analysis parameters in the literature. To avoid this, solidification parameters used in the present work are given in Table 2.

Microstructural evaluations

All samples were sectioned horizontally through the place that the tip of the thermocouples was located and prepared

Fig. 1 Dimensions of circulated water mold (units in mm)
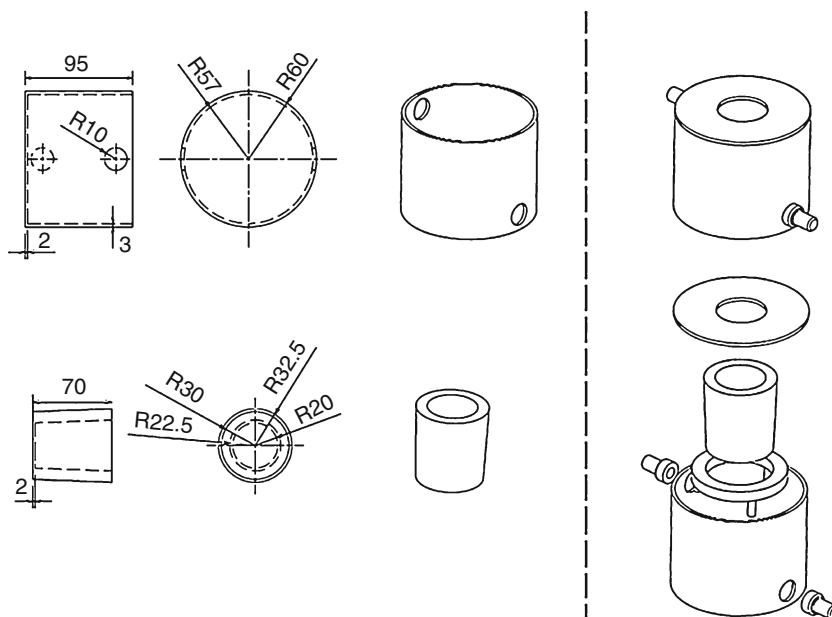
Table 2 Solidification characteristic parameters are shown in Fig. 2

Characteristic symbols	Characteristic description
$T_{N,\alpha}$	α-Al dendrite nucleation temperature
ΔT_u	Liquidus undercooling temperature ($=T_{Arrest} - T_{Min,\alpha}$)
ΔT_s	Range of solidification ($=T_{N,\alpha} - T_s$)
C.R	Cooling rate in mushy zone
$\Delta T_{R,\alpha}$	Recalescence undercooling temperature ($=T_G - T_{Min,\alpha}$)
$T_{Min,\alpha}$	α-Al dendrite minimum temperature
T_{Arrest}	Turning point of cooling curve ($d^2T\, dt^{-2} = 0$)
$T_{G,\alpha}$	α-Al dendrite growth temperature
T_s	Solidus temperature (end of solidification)
t_f	Total solidification time

for metallographic study. They were mechanically polished and then etched for metallographic observations. Keller's reagent (5 mL hydrofluoric acid, 10 mL hydrochloric acid, 20 mL nitric acid, and 65 mL water) was used for microstructural study. The prepared surfaces were studied using a Unimet optical microscope. Furthermore, to measure dendrite arm spacing, Clemex vision PE 3.5 software (Clemex Technologies Inc., Longueil, Quebec, Canada) was used.

Results and discussion

Thermal analysis parameters

Thermal analysis parameters which were analyzed in the present study are illustrated in Fig. 2. As seen, the liquidus region is magnified to indicate clearly the various parameters analyzed, and how they are measured from the thermal analysis curve. In this research, cooling rate is calculated from the slope of the line portion between the liquidus and eutectic regions. According to Gruzleski and coworkers [18] investigation, nucleation temperature is obtained from the second derivative curve. When solidification process starts by nucleation of primary α-Al dendrites, a quantity of second derivative ascends quickly, and detectable peak related to start of solidification appears in the second derivative curve. Nucleation temperature of primary α-Al dendrites is coincidence on minimum point of the valley just before the perceptible peak which is related to the starting point of solidification in the second derivative curve. This point is demonstrated in Fig. 2. Increasing the amount of second derivative at start point of solidification is in accordance with variation of slope of the line at first derivative curve. At first derivative curve, by starting the solidification process, the slope of the line is changed, and the first derivative quantity gets more positive value. Increasing in both second and first derivative curves is related to the amount of latent heat which is released during formation of first solid phase nuclei in molten metal. Therefore, some researchers used the first derivative curve to detect the nucleation temperature instead of the second derivative curve [5, 8]. Although detecting of nucleation temperature using the second derivative curve has a negligible error, detecting of the variation of slope at the first derivative curve is more difficult and needs high accuracy equipment. Since by smoothing operation, changing in slope of the line can be fade, this operation can have some effects on detecting the nucleation temperature via the first
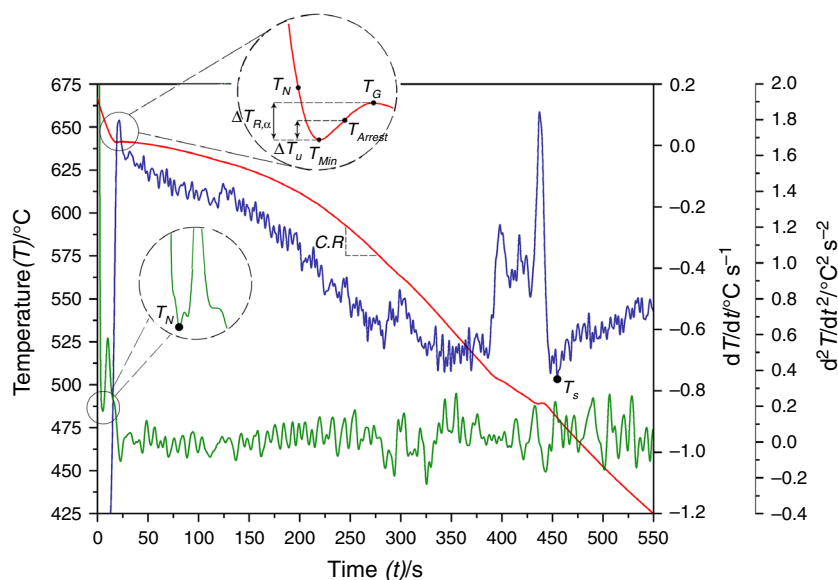
derivative curve. In the most literature, finishing point of solidification is achieved from the first derivative curve [18–22]. This parameter is obtained from the first minimum point of this curve after the last sensible peak related to end of solidification in the first derivative curve. These parameters are shown in Fig. 2. The cooling rates obtained for the various experimental conditions range from 0.4 to 17.5 °C s^{-1}.

Effect of cooling rate on solidification parameters

The cooling curves recorded for Al2024 alloy at various cooling rates are illustrated in Fig. 3. The first peak in the cooling curve represents the formation of aluminum primary phase, and the second is related to eutectic phase formation. As seen in this Figure, formation temperatures of the various phases are changed when the cooling rate is changed. The cooling rate is related to the heat extraction from the sample during solidification [23]. At low cooling rate, the rate of heat extraction from the sample is slow, and the slope of the cooling curve is small. But at high cooling rate condition, the rate of heat extraction is fast, and the slope of the cooling curve is steep. By increasing the cooling rate, the cooling curve is shifted to narrow time intervals. Also, observation of peaks in the cooling curve becomes more difficult, at high cooling rates. The cause of this event is, where the cooling rate is increased, released latent heat of the phase reaction is extracted from the system quickly. So, the reaction peak is occurred in smaller time interval.

The effect of cooling rate on the nucleation temperature (liquidus temperature) and solidus temperature of Al2024 alloy is illustrated in Figs. 4 and 5. As the cooling rate increases from 0.4 to 17.5 °C s^{-1}, the nucleation
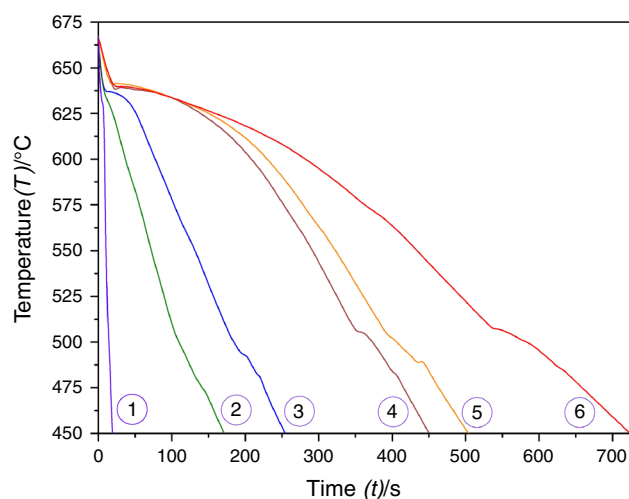
Fig. 3 Effect of different cooling rates on cooling curve of Al2024: *1* 15.41, *2* 2.46, *3* 1.14, *4* 0.74, *5* 0.65, *6* 0.42 (units in °C s^{-1})

temperature decreases from 643.1 to 635.7 °C, and solidus temperature reduces from 489.0 to 457.9 °C. This is in accordance with Backerud et al. and Samuel et al. [11, 24] investigations. The main reason for this event is probably related to the kinetics of diffusion in both liquid and solid states. According to Porter and Shewmon researches, when molten metal is cooled from above the liquidus temperature, increasing the cooling rate causes deviation of liquidus and solidus lines from their equilibrium lines [25, 26]. Since the rate of diffusion in liquid state is intrinsically high, this deviation in liquidus line is approximately negligible. As a result, by increasing the cooling rate, both liquidus and solidus temperature are decreased, and this reduction is higher in solidus line.
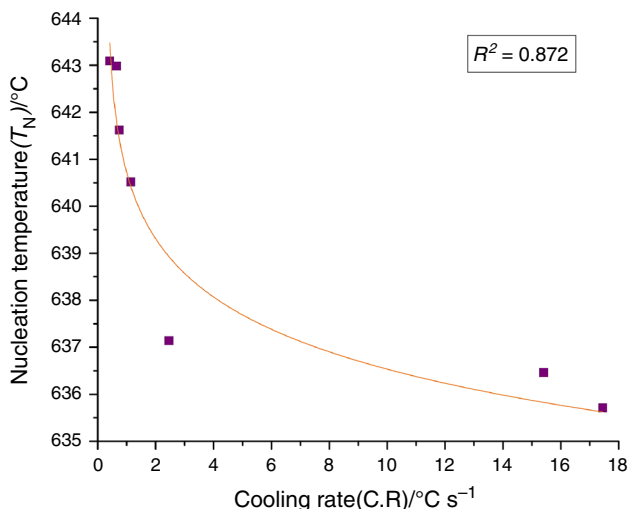
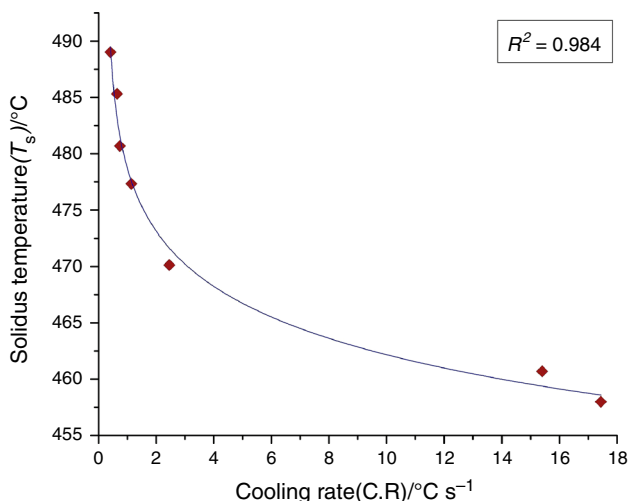**Fig. 4** Nucleation temperature versus cooling rate in Al2024

Fig. 5 Solidification temperature versus cooling rate in Al2024

Table 3 The effect of cooling rate on the liquidus and recalescence undercooling temperature

Cooling rate/°C s^{-1}	0.418	0.648	0.744	1.14
ΔT_{U}/°C	0.067	0.153	0.414	0
$\Delta T_{R,\alpha}$/°C	0.143	0.320	0.912	0

temperatures are clearly shown in Fig. 2. Undercooling parameters are only observed in low cooling rates. In medium and high cooling rates (higher than 2 °C s^{-1}), the latent heat of primary α-Al formation is released and extracted from the system very fast. In these conditions, the first derivative curve does not intersect the dT/dt = 0 line. Therefore, T_{Min}, T_{Arrest}, and T_{G} could not be calculated.

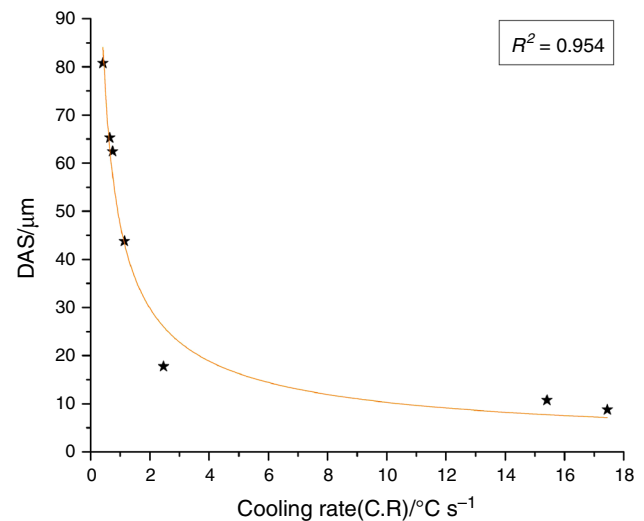The effect of cooling rate on the liquidus and recalescence undercooling temperature of Al2024 alloy, ΔT_{U}, and $\Delta T_{R,\alpha}$ is given in Table 3. As seen in this Table, by increasing the cooling rate, these parameters increase initially and then decrease at higher cooling rates. This behavior shows a very resemblance to the Charbonnier investigation, where the $\Delta T_{R,\alpha}$ is correlated with the grain size of the casting [29]. Also, similar behavior of ΔT_{U} parameter is represented by Gowri et al. [30] in other experiments.

According to some literature, there is a critical amount of cooling rate, in which, ascendant behavior of ΔT_{U} and $\Delta T_{R,\alpha}$ characteristic is changed to decrease [24, 29, 30]. The main reason for undercooling enhancement in the first stage is not clearly presented to now. But it can be related to thermal saturating of the molten metal. In low cooling rates, the rate of latent heat releasing is higher than the heat extraction rate from the system. This event causes thermal saturating of the melt. After the critical cooling rate, the reason of decreasing ΔT_{U} and $\Delta T_{R,\alpha}$ is related to the heat extraction rate from the melt. By increasing the cooling rate, the influence of extraction heat rate becomes dominant. In this condition, existing nuclei in the melt become more activated, and the growth condition is facilitated.

The influence of cooling rate on total solidification time, t_{f}, and the range of solidification temperature, ΔT_{s}, are illustrated in Figs. 6 and 7, respectively. Most investigations were focused on these parameters. By increasing the cooling rates, the slope of cooling curve becomes steeper. All of the reactions occur in a shorter time intervals, and total solidification time is decreased. This variation is shown in Fig. 3, too. As presented in this paper, both nucleation temperature and finish point of solidification are decreased by cooling rate enhancement. But, this decrease is more intensive in solidus line. Therefore, the resultant which is the range of solidification temperature becomes more extensive.

But some researchers have observed the enhancement of nucleation temperature by increasing the cooling rate [21–23, 27, 28]. They present that the solidification rate depends on the mobility of clusters of atoms in the melt. In this point of view, increasing the cooling rate increases the heat extraction, and the melt is cooled to a lower temperature than the equilibrium melting point. This condition causes the increasing of potential substrates to nucleate.

Liquidus undercooling temperature of Al2024 alloy, ΔT_{U}, is the difference between the turning point of cooling curve, T_{Arrest}, and minimum temperature, T_{Min} and recalescence undercooling temperature, $\Delta T_{R,\alpha}$, is the difference between growth temperature, T_{G}, and T_{Min}. These

Fig. 6 Effect of cooling rate on solidification time in Al2024

Fig. 8 Dendrite arm spacing versus cooling rate in Al2024
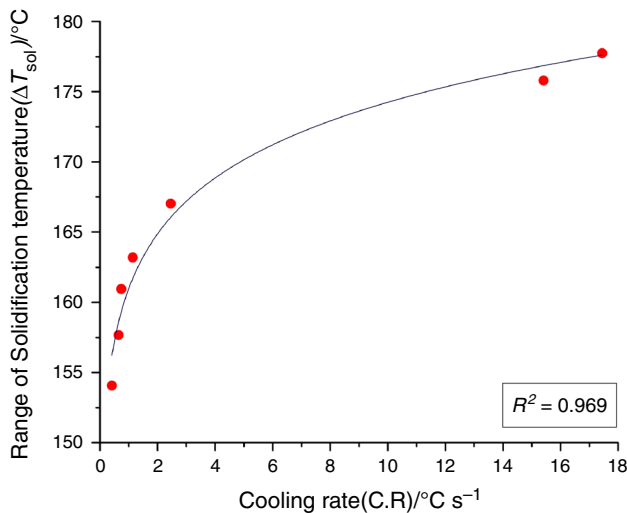
Fig. 7 Effect of cooling rate on range of solidification temperature in Al2024

Effect of cooling rate on dendrite arm spacing

Figure 8 indicates the effect of the cooling rate on dendrite arm spacing of Al2024 alloy. As seen, increasing the cooling rate from 0.4 to 17.5 °C s^{-1} decreases the DAS about 89 per cent. In the highest cooling rate, the DAS is fine (≈ 8.75 μm). For the sample cooled with lowest cooling rate, the DAS is large (≈ 80.73 μm). The mechanical properties of the aluminum alloys are strongly dependent on DAS. Changing in DAS as a function of cooling rate may arise from two reasons [21, 31–33]:

1. By increasing the cooling rate, atoms mobility in solid–liquid interface increases and causes the increase

in surface to volume ratio of dendrites. Therefore, it causes dendrite arm spacing to be reduced. On the other hand, since the cooling rate is high, time range in diffusion process is narrow, and the response of the system to this situation is to reduce diffusion path (dendrite arm spacing) and to enhance the surface of dendrites.

2. Because of the short solidification time and low velocity of diffusion at high cooling rates, growth velocity of dendrite is low. In this solidification condition, fine dendritic structure is the resultant.

As seen in Fig. 8, the correlation between DAS and cooling rate is in an exponential mode. The relation between DAS and cooling rate was represented for many alloys by Backerud, Flemings, Gruzleski, Shabestari, and other researchers [11, 13, 16, 21, 23]. But most of these investigations have been done on cast aluminum alloys. The following relation between DAS and the cooling rate for Al2024 can be presented as

$$\text{DAS} = 46.51(\text{C.R})^{-0.59} \tag{1}$$

where DAS is the dendrite arm spacing in micrometers, and C.R is the cooling rate in °C s^{-1}. By measuring DAS using a typical metallography and applying Eq. (1), the cooling rate can be calculated in each section of 2024 aluminum alloy in the intricate shapes.

Microstructural evaluations

Microstructure of Al2024 alloy in some cooling rates is demonstrated in Fig. 9. The microstructure of this alloy contains α-Al dendrites, Al$_2$Cu, Mg$_2$Si, Al$_2$CuMg, and

Fig. 9 Microstructure of Al2024 in different cooling rates: **a** 0.42, **b** 0.65, **c** 0.74, **d** 1.14, **e** 2.46, **f** 15.41, **g** 17.45 (units in °C s^{-1})
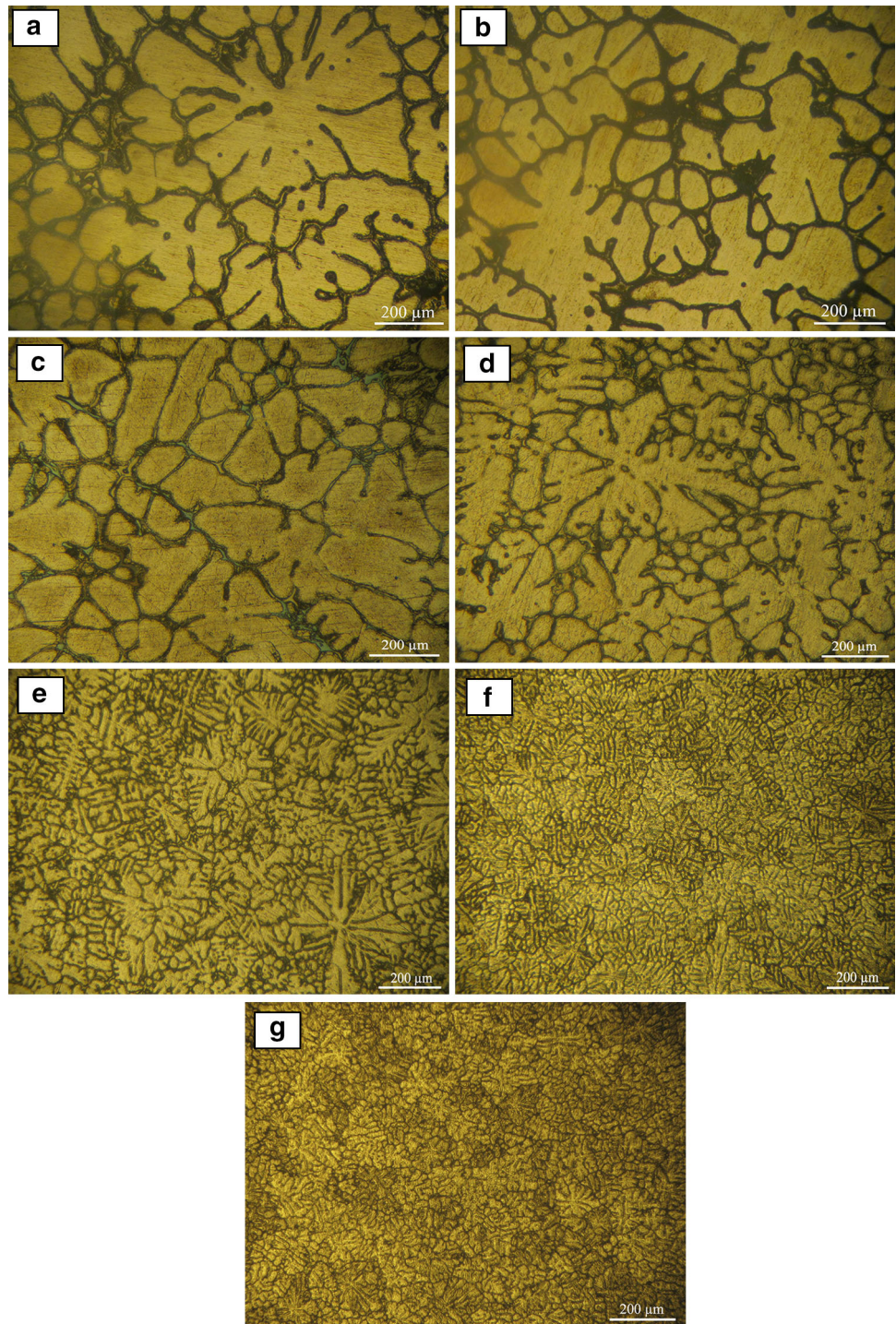
some complicated intermetallics. Dendrite arm spacing has been decreased, and intermetallics compounds have been refined in Al2024 alloy by increasing the cooling rate. Refining of dendrite arms is caused by

1. When the cooling rate increases, the amount of potential substrates for nucleation of primary α-Al phase is increased. Therefore, the fraction of nucleated primary dendrites enhances in constant volume of the molten metal. This event causes refining of dendrites structure and decreasing the dendrite arm spacing.

2. Effect of cooling rate on dendrite arm spacing is controlled by kinetics of diffusion and solidification time. Therefore, at higher cooling rates, the growth of dendrite arms stars quickly, and dendrite arm spacing is decreased.

Table 4 Correlation between solidification parameters in aluminum 2024 alloy (temperature/°C, cooling rate/°C s^{-1}, DAS/µm)

Solidification parameters	Equation
Nucleation temperature vs. cooling rate	$T_N = -1.59\ln(C.R-0.29) + 640.16$
Solidus temperature vs. cooling rate	$T_S = -6.31\ln(C.R-0.29) + 476.52$
Solidification time vs. cooling rate	$T_f = 270.60(C.R)^{-0.94}$
Range of solidification temperature vs. cooling rate	$\Delta T_{sol} = 160.98(C.R)^{0.03}$
Dendrite arm spacing vs. cooling rate	$DAS = 46.51(CR)^{-0.59}$

Increasing the cooling rate refines all intermetallic compounds and creates a uniform distribution of them in the microstructure.

The correlation between different solidification characteristics of 2024 aluminum alloy is given in Table 4. These equations may be used to study the solidification behavior of molten Al2024 alloy. It can also be used in physical simulation of Al2024 solidification at different cooling rates such as direct-chill casting process.

Conclusions

The effect of cooling rate on microstructure and solidification characteristics of 2024 aluminum alloy such as undercooling temperature, nucleation and solidification temperatures, and DAS were studied. The results are summarized as follows:

1. Solidification characteristics are influenced by the cooling rate. The temperature of various phases reactions is shifted to shorter time intervals with an increasing the cooling rate.
2. Increasing the cooling rate decreases significantly both nucleation temperature and finish point of solidification. Also, solidification time is decreased, and the range of solidification temperature is increased by cooling rate enhancement.
3. By increasing the cooling rate, both liquidus undercooling temperature and recalescence undercooling temperature initially increase and after reaching the summit, go downward.
4. The plot of DAS as a function of the cooling rate shows an exponential relationship. Increasing the cooling rate from 0.4 to 17.5 °C s^{-1} decreases DAS about 89 %. A numerical correlation between the cooling rate and DAS is calculated for Al2024 alloy.
5. Increasing the cooling rate refines all microstructural features including dendrite cells, DAS, and intermetallic compounds.

References

1. Kaufman JG. Introduction to aluminum alloys and tempers. 1st ed. Materials Park: ASM International; 2000.
2. Kissell JR, Ferry RL. Aluminum structures. 2nd ed. New York: Wiley; 2002.
3. Nadella R, Eskin DG, Du Q, Katgerman L. Macrosegregation in direct-chill casting of aluminum alloys. Prog Mater Sci. 2008;53:421–80.
4. Eskin DG. Physical metallurgy of direct chill casting of aluminum alloys. 1st ed. Boca Raton: Taylor & Francis Group; 2008.
5. Djurdjevic MB, Huber G, Odanovic Z. Synergy between thermal analysis and simulation. J Therm Anal Calorim. 2013;111:1365–73.
6. Emadi D, Whiting LV, Nafisi S, Ghomashchi R. Applications of thermal analysis in quality control of solidification processes. J Therm Anal Calorim. 2005;81:235–42.
7. Brown ME, Gallagher PK. Handbook of thermal analysis and calorimetry, vol. 5. 1st ed. Amsterdam: Elsevier B.V; 2008.
8. Malekan M, Shabestari SG. Computer aided cooling curve thermal analysis used to predict the quality of aluminum alloys. J Therm Anal Calorim. 2010;103:453–8.
9. Backerud L, Sigworth GK. Recent development in thermal analysis of aluminum casting alloys. AFS Trans. 1989;97:459–64.
10. Mahfoud M, Prasada Rao AK, Emadi D. The role of thermal analysis in detecting impurity levels during aluminum recycling. J Therm Anal Calorim. 2010;100:847–51.
11. Backerud L, Krol E, Tamminen J. Solidification characteristics of aluminum alloys, vol. 1. 1st ed. Oslo: Skan Aluminum; 1986.
12. Flemings MC. Solidification processing. 1st ed. New York: McGraw-Hill; 1974.
13. Apelian D, Sigworth GK, Whaler KR. Assessment of grain refinement and modification of Al–Si foundry alloys by thermal analysis. AFS Trans. 1984;91:297–307.
14. Kurz W, Fisher DJ. Fundamentals of solidification. 3rd ed. Aedermannsdorf: Trans Tech Publication Ltd; 1989.
15. Cruz KS, Meza ES, Fernandes FAP, Quaresma JMV, Casteletti LC, Garcia A. Dendrite arm spacing affecting mechanical properties and wear behavior of Al–Sn and Al–Si alloys directionally solidified under unsteady-state conditions. Metall Mater Trans A. 2010;41:972–84.
16. Flemings MC, Kattamis TZ, Bardes BP. Dendrite arm spacing in aluminum alloys. AFS Trans. 1991;99:501–6.
17. Easton M, Davidson C, StJohn D. Effect of alloy composition on the dendrite arm spacing of multicomponent aluminum alloys. Metall Mater Trans A. 2010;41:1528–38.
18. Gloria D, Gruzleski JE. Time as a control parameter in determination of grain size of 319 Al–Si–Cu foundry alloy. AFS Trans. 1999;107:419–24.
19. Dedavid BA, Costa EM, Ferreira CR. A study of precipitates formation in AA 380.0 aluminum alloys modified by the addition of magnesium. J Therm Anal Calorim. 2002;67:473–80.
20. Farahany S, Ourdjini A, Idris MH, Shabestari SG. Computer-aided cooling curve thermal analysis of near eutectic Al–Si–Cu–Fe alloy. J Therm Anal Calorim. 2013;114:705–17.
21. Shabestari SG, Malekan M. Thermal analysis study of the effect of the cooling rate on the microstructure and solidification parameters of 319 aluminum alloy. Can Metall Q. 2005;44:305–12.

22. Mackay RI, Djurdjevic MB, Sokolowski JH. Effect of cooling rate on fraction solid of metallurgical reactions in 319 alloy. AFS Trans. 2000;108:521–30.

23. Shabestari SG, Malekan M. Assessment of the effect of grain refinement on the solidification characteristics of 319 aluminum alloy using thermal analysis. J Alloys Compd. 2010;492:134–42.

24. Gowri S, Samuel FH. Effect of cooling rate on the solidification behavior of Al-7 Pct Si-SiC$_p$ metal–matrix composites. Met Trans A. 1992;23:3369–76.

25. Porter DA, Easterling KE. Phase transformation in metals and alloys. 2nd ed. London: Chapman & Hall; 1991.

26. Shewmon PG. Diffusion in solids. 1st ed. New York: McGraw-Hill; 1963.

27. Hosseini VA, Shabestari SG, Gholizadeh R. Study of the cooling rate on the solidification parameters, microstructure, and mechanical properties of LM13 alloy using cooling curve thermal analysis technique. Mater Des. 2013;50:7–14.

28. Malekan M, Dayani D, Mir A. Thermal analysis study on the simultaneous grain refinement and modification of 380.3 aluminum alloy. J Therm Anal Calorim. 2013;. doi:10.1007/s10973-013-3189-x.

29. Charbonnier J. Microprocessor assisted thermal analysis testing of aluminum alloy structures. AFS Trans. 1984;92:907–22.

30. Gowri S. Comparison of thermal analysis parameters of 356 and 359 alloys. AFS Trans. 1994;102:503–8.

31. McCartney DJ, Hunt JD. Measurements of cell and primary dendrite arm spacing in directionally solidified aluminum alloys. Acta Metall. 1981;29:1851–63.

32. Young KP, Kirkwood DH. The dendrite arm spacing of aluminum–copper alloys solidified under steady-state conditions. Metall Trans A. 1975;6:197–205.

33. Sivarupan T, Caceres CH, Taylor JA. Alloy composition and dendrite arm spacing in Al–Si–Cu–Mg–Fe alloys. Metall Mater Trans A. 2013;44:4071–80.